High-order Raman scattering mediated by self-trapped exciton in halide double perovskite

Kai-Xuan Xu,[1,2,*] Jia-Min Lai,[1,2,*] Yuan-Fei Gao,[3] Feilong Song,[3] Yu-Jia Sun,[1,2] Ping-Heng Tan,[1,2] and Jun Zhang[1,2,4,†]

[1]*State Key Laboratory of Superlattices and Microstructures, Institute of Semiconductors, Chinese Academy of Sciences, Beijing 100083, China*

[2]*Center of Materials Science and Optoelectronics Engineering, University of Chinese Academy of Sciences, Beijing 100049, China*

[3]*Beijing Academy of Quantum Information Sciences, Beijing 100193, China*

[4]*CAS Center of Excellence in Topological Quantum Computation, University of Chinese Academy of Sciences, Beijing 100049, China*

(Received 1 April 2022; accepted 9 August 2022; published 22 August 2022)

High-order Raman scattering is a typical photophysical process in understanding the electron–phonon coupling (EPC) in materials. In a "soft" polar lattice, due to the strong EPC, the excited electron-hole pairs can be captured by the lattice deformation potential, forming the self-trapped exciton (STE). Although high-order Raman scattering mediated by STE has been predicted by theory, there are rare experimental reports, especially in the double perovskite $Cs_2Ag_{0.4}Na_{0.6}InCl_6$, with highly efficient white light emission. We observed high-order Raman mode up to 12 orders at 4 K in $Cs_2Ag_{0.4}Na_{0.6}InCl_6$ by resonance excitation. We propose a physical picture of high-order Raman scattering mediated by STE to explain well the linear dependence of frequency and linewidth with order number. A reduction in the EPC with a temperature increase is attributed to the breakdown of momentum conservation during high-order scattering and the delocalization of the STE. Our work deepens the understanding of the EPC in STE and inspires the research of the excited-state decay process.

DOI: 10.1103/PhysRevB.106.085205

I. INTRODUCTION

The decay process of excited electrons in matter is important for understanding fundamental optical physics and designing high-performance optoelectronic devices such as lasers [1–3], light-emitting diodes [4], and solar cells [5–7]. Besides the nonradiative process, the excited electrons can decay to the ground state either through radiation or scattering, in which electron–phonon interaction is essential for determining the efficiency of light emission [8,9] and light harvesting [10]. Particularly, in resonance excitation near the Van Hove critical points of the electronic band or exciton state, the multiphonon process prominently dominates the decay process [11–13] and leads to very interesting spectral features with broadband phonon sideband emission or high-order Raman peaks. These phonon-involved decay processes and corresponding electron–phonon coupling (EPC) have been widely studied and evaluated in theory and experiments by analyzing the phonon-related fine structure of photoluminescence (PL) [14–18] and high-order Raman scattering spectroscopy [19–23]. One example of the typical broadband phonon–sideband emissions is the F center (Farbe center) usually found in alkali halide compounds [24,25] such as NaCl and KBr, in which an anionic vacancy in a crystal lattice is occupied by one or more unpaired electrons. Electrons in such a vacancy tend to absorb light in the visible spectrum so that a material that is usually transparent becomes colored. In 1950, Huang and Rhys first proposed the multiphonon transition theory based on the Franck–Condon principle to explain the broad absorption and emission spectra observed in the F center, and quantitatively evaluated the EPC strength by the Huang-Rhys factor S [17]. In 1959, Hopfield [15] used the Huang-Rhys theory to explain the Poisson distribution of discrete multiphonon spectral lines in CdS. When the EPC is strong enough in a "soft" lattice insulator, the excited electrons will be trapped by a potential well that is produced by local lattice distortion and will form self-trapped excitons (STEs), which has been reported in many materials [26–29], such as halogen crystals, condensed rare gases, organic molecular crystals, and perovskites. In these STE materials, multiphonon-involved decay of excited electrons plays an important role in the determination of their optical properties. The PL spectrum of STEs usually shows a large Stokes shift and broad linewidth below the band gap that reflects the multiphonon levels of the electronic ground states [16,18]. The EPC strength S can be obtained from the full width at half maximum (FWHM) [30,31] or Stokes shift [14] of luminescence. However, it is difficult to distinguish which phonon mode dominates the formation of STEs.

In contrast to PL spectra, high-order Raman scattering not only can reveal EPC, but also can specify the phonon modes that contribute to the formation of STEs. The theory of high-order Raman scattering mediated by STEs was given by Shorygin [32] and Allen and Perebeinos [33,34]. Despite several experimental reports of high-order Raman scattering mediated by STE states [35–37], a clear physical picture is still lacking. In recent years, Na-doped $Cs_2AgInCl_6$ halide perovskite with STEs has become a hotspot in fundamentals and applications due to their broad emission spectra covering the visible light range and their high external quantum efficiency [16]. However, direct observation of the high-order Raman scattering process mediated by STEs in Na-doped

*These authors contributed equally to this work.
†zhangjwill@semi.ac.cn

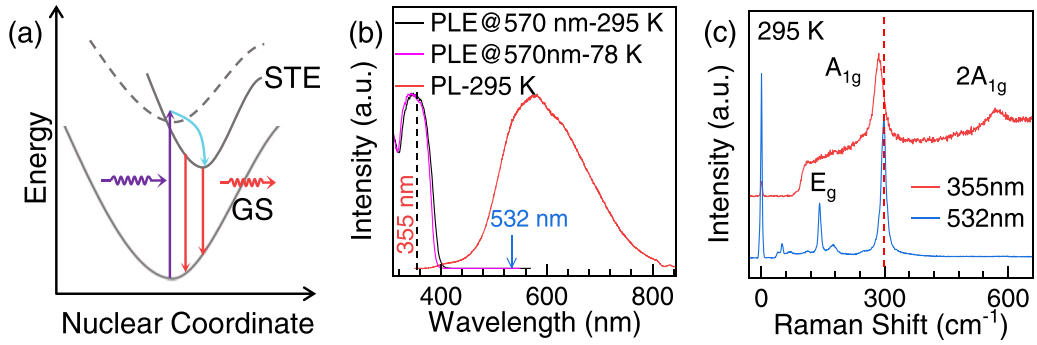

FIG. 1. Self-trapped exciton formation and Raman scattering for $Cs_2Ag_{0.4}Na_{0.6}InCl_6$. (a) The formation principle of the STE state (GS = ground state). (b) The PL spectrum ($\lambda_{exc} = 355$ nm) and photoluminescence excitation (PLE) spectra ($\lambda_{em} = 570$ nm) of $Cs_2Ag_{0.4}Na_{0.6}InCl_6$. The excitation wavelengths for Raman scattering spectroscopy are marked. (c) The Raman spectra of $Cs_2Ag_{0.4}Na_{0.6}InCl_6$ excited by a 355-nm and 532-nm laser at 295 K.

$Cs_2AgInCl_6$ has not been reported so far. Here, we report the high-order Raman scattering up to 12-order A_{1g} modes in $Cs_2Ag_{0.4}Na_{0.6}InCl_6$ at 4 K. We propose a physical picture of high-order Raman scattering mediated by STEs to explain well the linear dependence of frequency and linewidth with the order number. We investigate temperature-dependent, high-order Raman scattering and estimate the strength of EPC by the intensity ratio of the second overtone and fundamental.

II. RESULTS AND DISCUSSION

The double perovskite $Cs_2Ag_{0.4}Na_{0.6}InCl_6$ with a small amount of Bi (0.04%, atomic ratio to In) has been reported with a high external quantum efficiency (~70%) via radiative recombination of STEs because Na alloying reduces the electronic dimensionality and breaks down the parity-forbidden transition [16]. In $Cs_2Ag_{0.4}Na_{0.6}InCl_6$, excited electrons can be trapped by the local deformation potential induced by lattice distortion and form STEs [16]. Figure 1(a) displays the generation process of STEs. The excited electrons relax to the bottom of the conduction band and are then trapped by the lattice potential through electron–phonon interaction, forming a lower excited state–STE state. As shown in Fig. 1(b), the STEs exhibit a broad emission spectrum resulting from the enhancement of the overlap among different vibration level wave functions [38]. The large Stokes shift between the emission spectrum and excitation–emission spectrum further proves that the luminescence originates from the STE, which avoids the reabsorption effect of emitted photons, resulting in the improvement of quantum efficiency. The generation of STEs requires the energy of the excitation laser to be larger than the band gap (~3.22 eV, 385 nm). To explore the effect of STE formation, we compare Raman spectra excited near resonance (~3.49 eV, 355 nm) and below the band gap (~2.33 eV, 532 nm) in Fig. 1(c). The double perovskite $Cs_2Ag_{0.4}Na_{0.6}InCl_6$ belongs to O_h point group [39]. According to the polarized Raman spectroscopy, we refer peaks at 142 cm^{-1}, 250 cm^{-1}, and 175 cm^{-1} to E_g mode, and 295 cm^{-1} to A_{1g} mode (Supplemental Material Fig. S1 [40]). We note that $2A_{1g}$ mode can only be observed at a 355-nm resonance excitation, implying the STE formation facilitates the observation of multiphonon peaks. Compared to the spectrum at 532 nm laser excitation, the frequency of A_{1g} mode shows a redshift at 355 nm laser excitation, which is a result of the phonon softening induced by polaron formation [41]. Because the formation of STEs may change the lattice structure symmetry, E_g mode becomes forbidden at the backscattering configuration with 355 nm laser excitation.

To study the electron–phonon interaction in $Cs_2Ag_{0.4}Na_{0.6}InCl_6$ further, we measured the temperature-dependent Raman spectra. With resonance excitation (355 nm), the fundamental longitudinal optical (LO) phonon of A_{1g} mode and its overtones up to 12 orders are resolved at 4 K [Fig. 2(a)], whereas only the fundamental phonon mode can be observed with 532 nm laser excitation at the range of 4 K to 295 K [Fig. 2(b)]. Therefore, we deduce that these multiphonon peaks originate from the mediation of STEs. The Raman spectrum excited by 355 nm at 4 K can be well fitted by Lorentzian profiles, as shown in Fig. 2(c). We found there is a weak shoulder near the overtones of A_{1g} mode, which may come from transverse acoustic and transverse

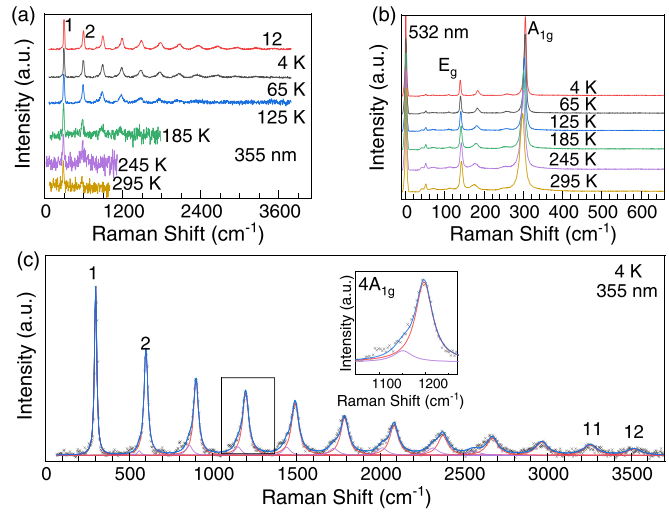

FIG. 2. Temperature-dependent Raman scattering spectra by resonance and nonresonance excitation. The Raman spectra at (a) a 355-nm resonance excitation and (b) a 532-nm nonresonance excitation from 4 K to 295 K. (c) Fitting results of resonance Raman spectrum with a 355-nm laser at 4 K. The inset shows the detail fitting result of $4A_{1g}$.

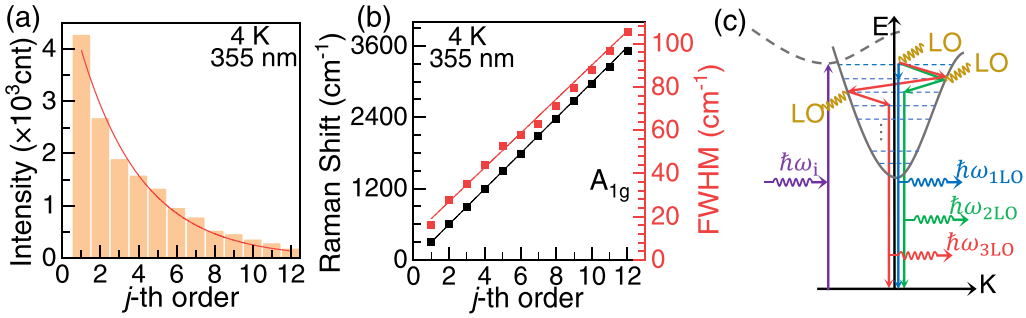

FIG. 3. Analysis of high-order Raman scattering in STE perovskite. (a) The intensity of overtones at 4 K. The solid red line is fitted by the function of $I = aP^j$, where P is the probability for scattering one phonon and a is the coefficient of intensity. (b) Frequency and FWHM of overtones at 4 K. The red and black solid lines are fitted by the linear function. (c) The schematic diagram of high-order Raman scattering process. The purple, blue, green, and red arrows denote incident laser ($\hbar\omega_i$) scattering light of 1LO, 2LO, and 3LO phonons, respectively.

optical phonon mode [42] from LO phonon attenuation or other activated phonons that are normally forbidden at nonresonance excitation [20,37]. In general adiabatic approximation, the Franck–Condon principle considers that electron transition leads to the displacement of nuclear coordinates [43], resulting in a small Stokes shift between the excited and ground states. While in STE, excited electrons coupled with phonons are described by the small polaron model, and the adiabatic approximation is no longer suitable. The formation of STEs results in a large Stokes shift and enhances the overlap between the vibrational wave function of the STE state and the ground state. Resonance excitation can largely enhance the scattering cross section, leading to increased scattering intensity [44]. In pioneering work, James Scott reported an empirical relationship that the order number of Raman modes is in proportion to the polaron coupling coefficients in semidconductors [45,46]. The increase of the observed order number implies EPC enhances with temperature decreases. Besides, temperature also affects the phonon dissipation induced by the anharmonic effect [47]. Low temperature contributes to the small phonon dissipation, thus the number of observed overtones increases with the temperature decreases. As a result, with the participation of STEs, we observed the LO mode up to 12 orders in resonance Raman spectra at 4 K.

We mainly discuss the origin of the multiphonon peaks. In previous work [20,37,48,49], two possible origins of the observed multiphonon process are the high-order Raman scattering and hot luminescence. In Raman scattering, electrons are excited to a virtual intermediate state (or a real state in resonance excitation), then transition back to the ground state [50] with absorbing or releasing phonons. However, in hot luminescence [48], the electrons absorb photons whose energy is larger than the band gap, becoming hot carriers in the conduction band. Then, the excited electrons relax along the excited state with phonon emission in cascade. After each phonon emission, the excited electrons have a probability of radiating back to the ground state. Therefore, the electron density of excited states determines the intensity of phonon emission peaks [48,51] which decays slowly as the order number increases. However, during high-order Raman scattering, the intensity of phonon peaks depends on the scattering probability; thus, the intensity of overtones is much smaller than that of the fundamental and can be fitted by $I = aP^j$, where P is the probability for scattering one phonon and a is the coefficient of intensity. The extracted intensity of multiphonon peaks at 4 K decays rapidly with the order number increases and can be well fitted with the exponential function, as shown in Fig. 3(a), where the scattering probability P is 0.73 ± 0.01. Thus, we consider that the observed multiphonon peaks in $Cs_2Ag_{0.4}Na_{0.6}InCl_6$ are attributed to the high-order Raman scattering.

Besides, the characteristic criteria of high-order Raman scattering also include the peak position and FWHM [20]. As shown in Fig. 3(b), the peak position can be fitted with a linear function $\omega_{j\mathrm{LO}} = j\omega_{\mathrm{LO}}$, where $\omega_{\mathrm{LO}} = 298.5 \pm 0.9\ \mathrm{cm}^{-1}$ is the frequency of the LO phonon, suggesting that the multiphonon peaks are contributed from the same phonon mode. Considering the requirement of momentum conservation, the dependence of linewidth on order number can be interpreted by the scattering process shown in Fig. 3(c): during 1LO phonon scattering, the excited electron is scattered to a virtual state by one phonon with wave vector $\boldsymbol{k} \sim 0$, and then the photons emit. Whereas during 2LO scattering, the excited electron is scattered to a real exciton state by a phonon with wave vector $\boldsymbol{k}_1 \neq 0$, and is then scattered back into the virtual state by the other phonon with wave vector $\boldsymbol{k}_2 = -\boldsymbol{k}_1$, followed by photon emitting. In 3LO phonon scattering, the electron is scattered twice to the real exciton state by phonons with wave vectors of $\boldsymbol{k}_1$ and $\boldsymbol{k}_2 = -2\boldsymbol{k}_1$, and is then scattered back into the virtual state by another phonon ($\boldsymbol{k}_3 = \boldsymbol{k}_1$). Therefore, the j-th order Raman scattering involves $(j-1)$ real electron states. Each time the phonon interacts with the real electron states, the linewidth increases with $\Delta\Gamma$. Therefore, the linewidth as a function of order number can be written as $\Gamma = \Delta\Gamma(j-1) + \Gamma_1$, where $\Gamma_1 \sim 19.0 \pm 1.2\ \mathrm{cm}^{-1}$ is the linewidth of the LO phonon, and $\Delta\Gamma \sim 7.9 \pm 0.2\ \mathrm{cm}^{-1}$. Similar linear temperature dependence of FWHM has been observed in CsI [20]. Based on these discussions, we further confirm the multiphonon process originates from the high-order Raman scattering.

Then, we discuss the temperature effect on EPC. Figures 4(a) and 4(b) displays the temperature-dependent Raman shift and linewidth of A_{1g} mode. The Raman shift can be fitted by a linear function with the slopes of $-0.05\ \mathrm{cm}^{-1}\ \mathrm{T}^{-1}$ at 355 nm laser excitation and $-0.02\ \mathrm{cm}^{-1}\ \mathrm{T}^{-1}$ at 532 nm laser excitation, which indicates the STE formation causes the frequency of the A_{1g} phonon to be more sensitive to

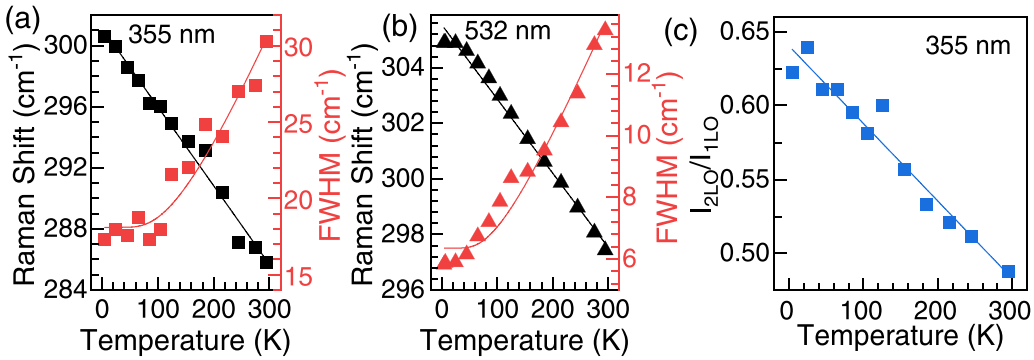

FIG. 4. Phonon anharmonic effect and scattering intensity ratio of 2LO phonon to 1LO phonon. Extracted Raman shift and FWHM of A_{1g} phonon with the increased temperature at (a) 355 nm laser excitation and (b) 532 nm laser excitation, respectively. (c) Temperature dependence of scattering intensity ratio of 2LO phonon to 1LO phonon. The solid line is fitted by linear function $I_{2LO}/I_{LO} = -5\times10^{-4}T + 0.64$.

the temperature. The anharmonic effect exists under both resonance and nonresonance excitation. In three-phonon anharmonic theory, the linewidth as a function of temperature can be written as [52]

$$\Gamma(T) = \Gamma_0[1 + 2/(e^x - 1)], \tag{1}$$

where $x = \hbar\omega_0/2kT$, Γ_0 is the FWHM at $T = 0$ K (18.1 ± 1.7 cm^{-1} for 355 nm laser excitation and 6.3 ± 0.2 cm^{-1} for 532 nm laser excitation), and k is the Boltzmann constant. As shown in Figs. 4(a) and 4(b), the redshift of the Raman peaks with elevated temperature is consistent with the effect of lattice thermal expansion. The linewidth increase of A_{1g} mode with elevated temperature is attributed to phonon–phonon interaction. The high-order Raman scattering process requires phonons to satisfy momentum conservation, which is easy to meet due to the small dissipation at low temperatures. The elevated temperature enhances the phonon anharmonic effect [53,54], which destroys momentum conservation. According to the model shown in Fig. 3(c), the elevated temperature increases phonon dissipation, destroying successive phonon scattering. Therefore, despite the population of phonons increasing, the number of phonon peaks we observed decreases at higher temperatures.

In addition, temperature also influences the localization of the excited electron and the strength of EPC. STE can be described by the Landau-Pekar model, which provides the dimensionless EPC of polaron α for the polar crystals [45]:

$$\alpha = e^2\left(\frac{1}{\varepsilon_\infty} - \frac{1}{\varepsilon_0}\right)\sqrt{\frac{m^*}{2\omega_{LO}}}, \tag{2}$$

where m^* is the band effective mass, ε_∞ and ε_0 are the static and high-frequency dielectric constant respectively, and ω_{LO} is the optical phonon frequency. With the temperature increasing, the dielectric constant and the phonon frequency are almost constants; thus, EPC is mainly determined by m^*. The elevated temperature makes the excited electrons span the potential barrier and disrupts the localization of STEs in the lattice [55]. In real space, the excited electrons are more localized at lower temperatures, corresponding to a more flat band structure near the center of the Brillouin zone, which leads to a larger effective mass and robust EPC. The Huang-Rhys factor S is an important dimensionless parameter to evaluate the strength of EPC in materials. Previous studies estimated EPC by radiative recombination of carriers and obtained an average value over the whole temperature range [16]. We use the same method to get a close value of the Huang-Rhys factor of 39 ± 5 (see Supplemental Material [40]). The soft and polar lattice of perovskite results in a strong EPC. In some hybrid materials, EPC would facilitate the fast nonradiative process, which decreases quantum efficiency [56]. However, in STE perovskite, the EPC—which is larger than that of hybrid perovskite—induces a large Stokes shift and avoids the emitted photon reabsorption, leading to the improvement of quantum efficiency. Here, we use the relative intensities of the second overtone and fundamental in Raman scattering spectra to evaluate the temperature dependence of EPC strength. As shown in Fig. 4(c), the value of the intensity ratio varies from 0.65 to 0.48 when the temperature increases from 4 K to 295 K, indicating that the strength of EPC is reduced, which is consistent with the weakening of exciton localization with the increasing temperature [57]. This is very different from the other non-STE materials, such as CdS [58,59] and Be-implanted GaN [60]. In these two typical semiconductors with strong EPC but without STE, the intensity ratio of the 2LO phonon to the 1LO phonon is independent of the temperature. This is because that STE is a new hybrid state called a small polaron due to the strong coupling between excitons and phonons. In small polarons, the coherent vibration of phonons dressed with excitons is enhanced at low temperatures [61]. As the temperature increases, the increased dissipation of phonons and excitons reduces the EPC. Note that the excitation energy, excitation power, detecting environments, etc., will affect the value of the EPC [62]. Therefore, the comparison of coupling strength needs to be carried out under the same measuring conditions.

III. CONCLUSION

Because of the strong EPC, we observed the STE state-mediated Raman scattering mode up to 12 orders in $Cs_2Ag_{0.4}Na_{0.6}InCl_6$ at 4 K. With the temperature increasing, reduction of the EPC is attributed to the breakdown of the momentum conservation during high-order scattering and the delocalization of the STE; thus, the order number of the observed phonon diminishes. Our findings can deepen the

understanding of the electron–phonon interaction in double perovskite with STE and promote the study of the excited-state decay process.

ACKNOWLEDGMENTS

J.Z. acknowledges the National Key Research and Development Program of China (Grant No. 2017YFA0303401); the CAS Interdisciplinary Innovation Team, National Natural Science Foundation of China (Grant No. 12074371); and the Strategic Priority Research Program of Chinese Academy of Sciences (Grant No. XDB28000000). We thank Prof. Jiang Tang and Dr. Jiajun Luo (Wuhan National Laboratory for Optoelectronics, School of Optical and Electronic Information, Huazhong University of Science and Technology) for providing the high-quality samples, as well as Prof. Shiwu Gao and Dr. Shengxiang Wu (Beijing Computational Science Research Center) for useful discussions.

[1] L. Lei, Q. Dong, K. Gundogdu, and F. So, Adv. Funct. Mater. **31**, 2010144 (2021).
[2] Q. Zhang, X. Liu, M. I. Utama, G. Xing, T. C. Sum, and Q. Xiong, Adv. Mater. **28**, 276 (2016).
[3] R. Roder, T. P. Sidiropoulos, C. Tessarek, S. Christiansen, R. F. Oulton, and C. Ronning, Nano Lett. **15**, 4637 (2015).
[4] J. Iveland, L. Martinelli, J. Peretti, J. S. Speck, and C. Weisbuch, Phys. Rev. Lett. **110**, 177406 (2013).
[5] Z. Yang *et al.*, Nat. Commun. **10**, 4540 (2019).
[6] W. Tian, R. Cui, J. Leng, J. Liu, Y. Li, C. Zhao, J. Zhang, W. Deng, T. Lian, and S. Jin, Angew. Chem. Int. Ed. Engl. **55**, 13067 (2016).
[7] P. O'Keeffe *et al.*, Nano Lett. **19**, 684 (2019).
[8] X. Sui *et al.*, Nano Lett. **21**, 4137 (2021).
[9] S. Peng, Q. Wei, B. Wang, Z. Zhang, H. Yang, G. Pang, K. Wang, G. Xing, X. W. Sun, and Z. Tang, Angew. Chem. Int. Ed. Engl. **59**, 22156 (2020).
[10] X. Gong *et al.*, Nat. Mater. **17**, 550 (2018).
[11] C. D. Dashwood *et al.*, Phys. Rev. X **11**, 041052 (2021).
[12] V. Perebeinos and P. Avouris, Phys. Rev. Lett. **101**, 057401 (2008).
[13] Q. Zhang, X. Liu, M. I. Utama, J. Zhang, M. de la Mata, J. Arbiol, Y. Lu, T. C. Sum, and Q. Xiong, Nano Lett. **12**, 6420 (2012).
[14] M. de Jong, L. Seijo, A. Meijerink, and F. T. Rabouw, Phys. Chem. Chem. Phys. **17**, 16959 (2015).
[15] J. J. Hopfield, J. Phys. Chem. Solids **10**, 110 (1959).
[16] J. Luo *et al.*, Nature (London) **563**, 541 (2018).
[17] K. Huang and A. Rhys, Proc. R. Soc. London A **204**, 406 (1950).
[18] K. Cho and Y. Toyozawa, J. Phys. Soc. Jpn. **30**, 1555 (1971).
[19] C. M. Iaru *et al.*, Nat. Commun. **12**, 5844 (2021).
[20] T. P. Martin, Phys. Rev. B **13**, 3617 (1976).
[21] T. P. Martin, Phys. Rev. B **11**, 875 (1975).
[22] F. Wang, W. Liu, Y. Wu, M. Y. Sfeir, L. Huang, J. Hone, S. O'Brien, L. E. Brus, T. F. Heinz, and Y. R. Shen, Phys. Rev. Lett. **98**, 047402 (2007).
[23] J. M. Lai, M. U. Farooq, Y. J. Sun, P. H. Tan, and J. Zhang, Nano Lett. **22**, 5385 (2022).
[24] M. Hirai, Y. Kondo, T. Yoshinari, and M. Ueta, J. Phys. Soc. Jpn. **30**, 440 (1971).
[25] W. C. Holton and H. Blum, Phys. Rev. **125**, 89 (1962).
[26] K. S. Song and R. T. Williams, *Self-Trapped Excitons* (Springer-Verlag, Berlin, 1993).
[27] R. T. Williams and K. S. Song, J. Phys. Chem. Solids **51**, 679 (1990).
[28] W. Tao, C. Zhang, Q. Zhou, Y. Zhao, and H. Zhu, Nat. Commun. **12**, 1400 (2021).
[29] Q. Zhang and X. Liu, J. Semicond. **40**, 090401 (2019).
[30] W. Stadler, D. M. Hofmann, H. C. Alt, T. Muschik, B. K. Meyer, E. Weigel, G. Muller-Vogt, M. Salk, E. Rupp, and K. W. Benz, Phys. Rev. B **51**, 10619 (1995).
[31] X. Lao, Z. Yang, Z. Su, Y. Bao, J. Zhang, X. Wang, X. Cui, M. Wang, X. Yao, and S. Xu, J. Phys. Chem. C **123**, 5128 (2019).
[32] P. P. Shorygin, Sov. Phys. Usp. **16**, 99 (1973).
[33] P. B. Allen and V. Perebeinos, Phys. Rev. Lett. **83**, 4828 (1999).
[34] V. Perebeinos and P. B. Allen, Phys. Rev. B **64**, 085118 (2001).
[35] J. Andreasson, J. Holmlund, C. S. Knee, M. Käll, L. Börjesson, S. Naler, J. Bäckström, M. Rübhausen, A. K. Azad, and S.- G. Eriksson, Phys. Rev. B **75**, 104302 (2007).
[36] J. Andreasson, J. Holmlund, R. Rauer, M. Käll, L. Börjesson, C. S. Knee, A. K. Eriksson, S.- G. Eriksson, M. Rübhausen, and R. P. Chaudhury, Phys. Rev. B **78**, 235103 (2008).
[37] J. A. Steele *et al.*, ACS Nano **12**, 8081 (2018).
[38] H. Tanino and K. Kobayashi, J. Phys. Soc. Jpn. **52**, 1446 (1983).
[39] G. Yang, Y. Zhu, X. Li, J. Huang, X. Xu, X. Ji, A. Wang, J. Cheng, and G. Pan, Opt. Lett. **46**, 6043 (2021).
[40] See Supplemental Material at http://link.aps.org/supplemental/10.1103/PhysRevB.106.085205 for the identification of phonon modes and for obtaining the Huang-Rhys factor *S*.
[41] A. Alexandrov and H. Capellmann, Phys. Rev. B **43**, 2042 (1991).
[42] X. Li, D. Liu, and D. Wang, Appl. Phys. Lett. **112**, 252105 (2018).
[43] M. Lax, J. Chem. Phys. **20**, 1752 (1952).
[44] P. Y. Yu and M. Cardona, *Fundamentals of Semiconductors: Physics and Materials Properties* (Springer Science & Business Media, Heidelberg, 2010).
[45] C. Franchini, M. Reticcioli, M. Setvin, and U. Diebold, Nat. Rev. Mater. **6**, 560 (2021).
[46] J. F. Scott, T. C. Damen, W. T. Silfvast, R. C. C. Leite, and L. E. Cheesman, Opt. Commun. **1**, 397 (1970).
[47] M. Kuball, J. M. Hayes, Y. Shi, and J. H. Edgar, Appl. Phys. Lett. **77**, 1958 (2000).
[48] R. M. Martin and C. M. Varma, Phys. Rev. Lett. **26**, 1241 (1971).
[49] Y. R. Shen, Phys. Rev. B **9**, 622 (1974).
[50] M. Cardona and R. Merlin, *Light Scattering in Solids IX* (Springer-Verlag, Berlin, 2006).
[51] C. Trallero-Giner and R. Riera, Phys. Status Solidi B **152**, 357 (1989).
[52] M. Balkanski, R. F. Wallis, and E. Haro, Phys. Rev. B **28**, 1928 (1983).
[53] H. Lengfellner and K. F. Renk, Phys. Rev. Lett. **46**, 1210 (1981).

[54] H. N. Liu, X. Cong, M. L. Lin, and P. H. Tan, Carbon **152**, 451 (2019).
[55] X. Wu, M. T. Trinh, D. Niesner, H. Zhu, Z. Norman, J. S. Owen, O. Yaffe, B. J. Kudisch, and X. Y. Zhu, J. Am. Chem. Soc. **137**, 2089 (2015).
[56] L. D. Whalley, P. van Gerwen, J. M. Frost, S. Kim, S. N. Hood, and A. Walsh, J. Am. Chem. Soc **143**, 9123 (2021).
[57] K. Shibata, J. Yan, Y. Hazama, S. Chen, and H. Akiyama, J. Phys. Chem. C **124**, 18257 (2020).
[58] R. C. C. Leite, J. F. Scott, and T. C. Damen, Phys. Rev. Lett. **22**, 780 (1969).
[59] K. Gong, D. F. Kelley, and A. M. Kelley, J. Chem. Phys **147**, 224702 (2017).
[60] W. H. Sun, S. J. Chua, L. S. Wang, and X. H. Zhang, J. Appl. Phys. **91**, 4917 (2002).
[61] S. Fratini and S. Ciuchi, Phys. Rev. Lett. **91**, 256403 (2003).
[62] Y. Yi, J. K. Marmon, Y. Chen, F. Zhang, T. Sheng, P. S. Wijewarnasuriya, H. Zhang, and Y. Zhang, Phys. Rev. Appl. **13**, 011001(R) (2020).